# Defect-mediated ferromagnetism in insulating Co-doped anatase $TiO_2$ thin films

K. Griffin Roberts,[1] M. Varela,[2] S. Rashkeev,[3,2,*] S. T. Pantelides,[3,2] S. J. Pennycook,[2,3] and Kannan M. Krishnan[1,†]
[1]*Department of Materials Science and Engineering, University of Washington, Seattle, Washington 98195, USA*
[2]*Materials Science and Technology Division, Oak Ridge National Laboratory, Oak Ridge, Tennessee 37831, USA*
[3]*Department of Physics and Astronomy, Vanderbilt University, Nashville, Tennessee 37235, USA*
(Received 2 June 2008; published 7 July 2008)

The nature of the defect responsible for room-temperature ferromagnetism in Co-doped anatase $TiO_2$ has remained elusive. Here we report atomic-resolution *Z*-contrast images of epitaxially grown $Co_{0.03}$:$TiO_2$ films showing that Co atoms are dispersed and occupy preferred interstitial sites. Density-functional calculations found that these sites are the lowest-energy configuration of Co in anatase and that O vacancies ($V_O$), introduced by annealing, anchor the Co atoms into Co-$Ti^{+3}$-$V_O$ complexes. The calculated magnetic moment is in agreement with our measured value and the calculated Co x-ray absorption spectrum is in agreement with data published in the literature.

DOI: 10.1103/PhysRevB.78.014409 PACS number(s): 75.70.−i, 71.15.Mb, 79.20.Uv, 85.75.−d

## I. INTRODUCTION

With the discovery of room-temperature ferromagnetism (RTFM) in Co-doped anatase $TiO_2$,[1] transition-metal (TM) doped oxides/nitrides have been a major focus in spintronics research.[2–8] However, many questions remain regarding the origin of ferromagnetism (FM), and its relationship with semiconducting properties and film microstructure in single-phase TM doped oxides. In particular, conventional FM theories in insulators[9] cannot explain their magnetism where the dopant concentration is well below the percolation threshold.[10] Similarly, theories of carrier-induced FM, such as the hole-mediated *p-d* exchange model[4] and the spin-split impurity band exchange model,[10] are not applicable to materials such as Co-doped anatase, which are FM yet highly insulating.[11–13]

Various reports highlight the important role of structural quality and either native[14] or dopant-introduced defects in activating RTFM in TM oxides.[11–17] Our previous work[11,18,19] on anatase Co:$TiO_2$, exhibiting weak RTFM in as-deposited form, shows an enhanced FM on postgrowth vacuum annealing. Related compositional analyses[11,19] show that the Co ions are homogeneously distributed in the lattice before and after annealing, eliminating the consideration of any magnetic impurity phases, and yet these films remain highly insulating. The activation of RTFM by the annealing process, which leads to the generation and migration of $V_O$'s and the diffusion of Co impurities, points to a defect-related mechanism. Theory has shown that dilute concentrations of lattice defects and impurity-defect complexes can produce a FM state in doped oxides e.g., Ca vacancies in $CaO_2$,[20] Hf vacancies in $HfO_2$,[21] and vacancy-impurity complexes in doped insulators.[22] Moreover, if specific impurity-defect complexes are responsible for such RTFM, it can be argued that the saturation moment would be independent of the Co-doping level. In fact, evidence in the literature[23] can be interpreted to mean that the saturation moment is independent of Co-dopant concentration. Specifically, in the Co:$TiO_2$ systems where experimental evidence has ruled out the possibility of metallic Co clusters, the observed FM has been attributed to (a) dispersed substitutional Co,[7] possibly with $V_O$'s,[24,25] (b) interstitial Co, with $V_O$'s playing no role,[26] or (c) high concentrations of substitutional Co.[27] While most of these studies[11–27] point to a FM mechanism associated with defects, the precise nature of the pertinent defect has not yet been established.

In this work we report a comprehensive study of epitaxially grown films of a single doping level of $Co_{0.03}$:$TiO_2$ using atomic-resolution *Z*-contrast imaging combined with electron-energy-loss spectroscopy (EELS). This enables us to determine accurately the Co concentration, ensure the absence of clusters or other Co phases, and image directly arrays of Co-$Ti^{+3}$-$V_O$ defect complexes in which Co atoms occupy select interstitial sites. For the processing conditions adopted here, these defects are seen only in annealed samples that are ferromagnetic at room temperature. First-principles, spin-polarized density-functional theory (DFT) calculations are used to confirm that these defects are preferred energetically over other configurations [the difference being of the order of 1–1.5 eV, as we will discuss later, and have a magnetic moment in agreement with the sample's measured value (within $\sim 0.25 \mu_B$/Co atom)]. Spin-aligning interactions appear to be sufficiently strong even in the dilute limit to account for FM ordering. Finally, calculated x-ray absorption spectra of Co in the Co-$Ti^{+3}$-$V_O$ defect are in agreement with published data[7] in single-phase Co-doped anatase but differ markedly from the spectrum of substitutional Co in anatase.

## II. EXPERIMENT

Films of anatase $Co_{0.03}$:$TiO_2$ were epitaxially grown by rf-magnetron sputter deposition on lattice-matched $LaAlO_3$(100) substrates to a film thickness of 100 nm. The base pressure of the sputter deposition chamber was $5 \times 10^{-7}$ torr and the films were grown in a pure Ar atmosphere at $4 \times 10^{-3}$ torr at a deposition rate of 0.01 nm/s. The films underwent a postgrowth annealing process in vacuum $<10^{-5}$ torr at 450 °C for 1 h. Both as-grown and annealed films were analyzed structurally by x-ray diffraction (XRD) and transmission electron microscopy (TEM), and were found to be of high structural quality, as reported

 

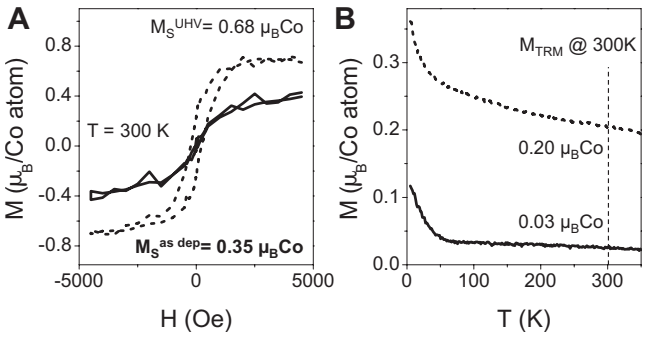


FIG. 1. (a) $M$ vs $H$ hysteresis loops measured at 300 K for the as-grown (solid line) and the UHV annealed (dotted line) $Co_{0.03}$:$TiO_2$ samples. (b) TRM curves taken from 5–365 K of as-deposited (solid line) and annealed (dashed line) films, illustrating the enhancement in magnetic properties with annealing. For TRM experiments, the sample is cooled to 5 K and saturated in a 1 T applied magnetic field; the field is then removed and the $M_{TRM}$, as a function of increasing temperature, is measured up to 365 K. TRM is useful as a direct measurement of the magnetic signal from the sample alone because the measurement is taken in zero applied field, and there is no contribution from the diamagnetic substrate. The increase observed below 50 K could point to a multiphase system, which could perhaps be related to the slight variations of Co distribution (always below 8%) observed in these samples (Ref. 19). Additionally, field cooled and zero-field cooled measurements of the same sample have revealed that the film exhibits no superparamagnetism; these results further support that there are no nanometer-scale metallic Co clusters present in the film, as these would contribute a peak in the zero-field cooled measurement. Note: Data adapted from Ref. 11. The moment per Co atom differs slightly from Ref. 11 because of a difference in Co concentration measurement (2% for Ref. 11, 3% here).

elsewhere.[11,18] Their magnetic properties [for hysteresis and $M$ vs $H$ at 300 K, see Fig. 1(a); for thermoremanent magnetization (TRM) and $M_{TRM}$ from 5–365 K, see Fig. 1(b)] were measured with a superconducting quantum interference device (SQUID) magnetometer. As shown in Fig. 1, the as-deposited film is weakly FM with a saturation magnetization $M_S$ of 0.15 $\mu_B$/Co atom, a coercivity $H_C$ of 100 Oe, and a $M_{TRM}$ at 300 K of 0.03 $\mu_B$/Co atom. The data shows that vacuum annealing at 450 °C yields an increase in $M_S$ to 0.65 $\mu_B$/Co atom, $H_C$ to 350 Oe, and $M_{TRM}$ to 0.20 $\mu_B$/Co atom (the $M_s$ value is somewhat different from that reported in Ref. 11 because the present method of measuring the Co concentration is more accurate). The Curie temperature was greater than the limit (>365 K) of the SQUID magnetometer. Both as-grown and annealed samples are highly insulating with resistivity $>10^6$ Ω cm. Moreover, the as-deposited film has an average oxygen content ~5 at % higher than the annealed film, confirming that the vacuum annealing process is reducing the oxygen and creating $V_O$'s. Finally, near-edge x-ray absorption fine-structure results on samples processed under identical conditions have confirmed Co to be uniformly in the +2 state.[11]

The STEM and EELS results reported here were obtained using aberration-corrected VG microscopes HB603U (300 kV) and HB501UX (100 kV). The HB501UX allows consecutive acquisition of EELS data with a Gatan Enfina spectrometer, and $Z$-contrast images to form spectrum images with a spatial resolution of 0.11 nm and an energy resolution below 0.5 eV.[28–31] Core-loss (EELS) spectrum images were taken at a number of locations and magnifications throughout the cross-sectional TEM specimens. Detailed compositional analysis (with better accuracy than our previous measurements reported in Ref. 11) using the Co and Ti $L$ edges (~779 and 455 eV, respectively, using hydrogenic cross sections including corrections for white lines), and the O $K$ edge (~530 eV, using a Hartree-Slater cross section) reveals that the Co is dissolved uniformly throughout the film thickness. The average Co/Ti ratio was calculated to be $0.030 \pm 0.03$ and $0.028 \pm 0.02$ for as-deposited and annealed samples, respectively. Both samples showed small spatial variations in Co maps with some increase in Co near the substrate-film interface and the top 20 nm of the film thickness with maximum Co concentration of 8 at %. The average oxygen content (atomic %) was calculated from the background subtracted O $K$ edge and normalized relative to the Ti content (calculated from the Ti $L$ edge). The details of the compositional analysis of a series of our Co:$TiO_2$ films are reported in Ref. 19. Although the structural analyses in Refs. 11 and 19 reveal the films to be of high crystalline quality, it is evident during the STEM imaging that the presence of structural defects such as grain boundaries and interfaces play a role in Co distribution. From this we determine that the Co concentration is not perfectly uniform throughout but is dispersed throughout the film thickness and has some correlation to the presence of structural defects. However, it is important to re-emphasize that no highly Co-enriched clusters or secondary phases were observed anywhere in the films of this report, including the grain boundaries.

## III. RESULTS AND DISCUSSION

Anatase has a body-centered tetragonal unit cell (lower inset of Fig. 2) and its epitaxial growth with high structural quality in the (100) orientation on the $LaAlO_3$ substrate was confirmed by high-resolution $Z$-contrast images (Fig. 2). The Ti/O columns, appearing as dumbbells, are the brightest while the O columns are dimmer and spaced between. Close inspection of the annealed Co-doped $TiO_2$ film specimen reveals a clear ordering in the O columns, resulting in a difference in intensity for neighboring O columns [see Fig. 3(a) and the intensity traces in Fig. 3(b)]. Furthermore, one of the two O columns of the annealed Co-doped $TiO_2$ sample [a in Fig. 3(a), and red arrows in Fig. 3(b)] is consistently brighter than the other adjacent column [b in Fig. 3(a) or blue arrows in Fig. 3(b)] in both the raw data and also after maximum entropy deconvolution [Fig. 3(a)]. This difference is too high to be explained in terms of a few oxygen vacancies in the dim columns. A more likely explanation is the presence of Co atoms either in or near the bright O columns. Indeed, a line trace of some of the brighter O columns shows a double peak [Fig. 3(b)]. This double peak structure is present only in the annealed Co-doped $TiO_2$ film, allowing us to conclude that it is due to Co atoms preferentially occupying a particular interstitial site. The ordering of Co ions is consistent throughout the annealed Co:$TiO_2$ film specimen. While at

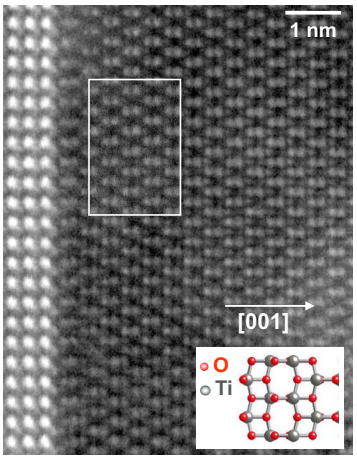


FIG. 2. (Color online) *Z*-contrast (high angle annular dark field) image of the annealed Co:$TiO_2$ film (right) on the LAO substrate (left). The image has been smoothed to remove noise (the upper inset shows the raw data). The lower inset shows a schematic of the anatase lattice with gray and red spheres representing Ti and O atoms, respectively, along the projection in the image.

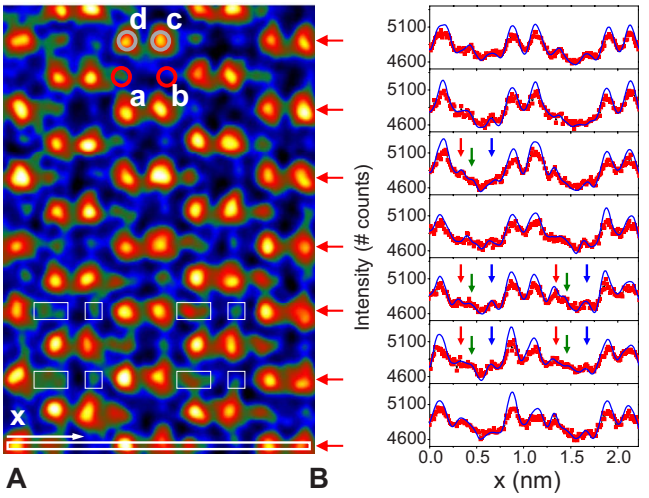


FIG. 3. (Color online) (a) Magnified image of the anatase lattice after maximum entropy deconvolution (from the same area as the upper inset of Fig. 2). The HREM Research Inc. plug in for digital micrograph was used, using a physical probe with a full width at half maximum of 0.071 nm. Red circles mark O columns while gray circles correspond to Ti/O columns. (The probe was simulated using the estimated aberration parameters convoluted with a Gaussian to account for the source size. The results are not sensitive to the exact probe shape used for the deconvolution.) (b) Intensity traces along the atomic planes marked with red arrows on (a), compared to traces from the raw image, before deconvolution. The blue lines represent an average of over five lateral pixels along boxes taken on the ME processed image, such as the white box on (a). The red dots represent the intensity traces from the same regions and averaged in the same way on the raw data image. It is seen that the bright O column actually comprises two peaks: one (red arrow) in the expected position for O and the another (green arrow) displaced away from the O column. This peak is due to preferential segregation of Co interstitials.

this point we cannot explain why the Co-$V_O$ complex chooses one of the O columns over the other one, the fact is that once it happens the order has long-range character. Long-range ordering of O vacancies is typical in perovskite-based structures such as Brownmillerite (see, for example, Ref. 32). The sample thickness for the microscopy experiments is 10–20 nm so the length scale of this ordering is longer than this value. Even though Co scatters about 50% more than Ti, our noise limit is around 10%. Therefore, it is possible that up to 20% of the total Co could be substitutional but would be undetectable. The possibility of the site ordering being due to lattice distortion from the $LaAlO_3$ substrate can be ruled out by the fact that both the as-deposited Co:$TiO_2$ films and the annealed, undoped $TiO_2$ films (both also grown on $LaAlO_3$) do not exhibit the O site ordering. As to why there is any RTFM in the as-deposited Co:$TiO_2$ films where we do not see the defect ordering—it is possible that some of the defect complexes are present but not in an ordered enough state for them to be detectable. Alternatively, the ordered domains may be smaller so that several domains of different polarity will be superimposed during the imaging, and consequently, the Co column would be less intense and could be invisible below the noise threshold. Also, the complexes may not be the only ones responsible for the RTFM. What we do know for a fact is that after the annealing, the RTFM is enhanced significantly when the extended ordered arrays of defects become visible. Most likely, the ordering helps to establish long-range FM correlations.

## IV. THEORY CALCULATIONS

To further analyze the data, we performed first-principles, spin-polarized DFT calculations using the generalized gradient approximation (GGA),[33] ultrasoft scalar relativistic pseudopotentials, and the VASP code[34] with supercells containing 120 host atoms. To address the disagreements in the literature,[26,27] we performed new calculations and found that the lowest-energy interstitial site is precisely the same as observed in the *Z*-contrast images. The interstitial Co was placed at a large number of interstitial sites and it always relaxed to the same site. Stable interstitial configurations that entail disruption of the network were also found but their energies are of order 1–1.5 eV higher.

Using the theory of Ref. 35 for the competition between interstitial and substitutional sites for an impurity, and the results of our total-energy calculations, we find that the interstitial-substitutional energy difference $\Delta E(I\text{-}S)$ for neutral defects is given by $\Delta E(I\text{-}S) = -0.8\ \text{eV} + kT \log p$, where $p$ is the partial pressure of $O_2$ molecules. Since $p \leq 1, \Delta E(I\text{-}S) < 0$, and interstitial Co is always preferred over substitutional Co.

In anatase, the Co interstitial breaks the tetragonal symmetry (Fig. 4): in the [010] projection the surrounding O atoms in the same row shadow the Co atom more efficiently than in the [100] projection. We find that two Co interstitials on the same O row in adjacent unit cells (down the O column) are energetically unfavorable, accounting for the absence of Co aggregation even after annealing. However, $V_O$'s are attracted to the Co interstitials with a Co-$V_O$ binding

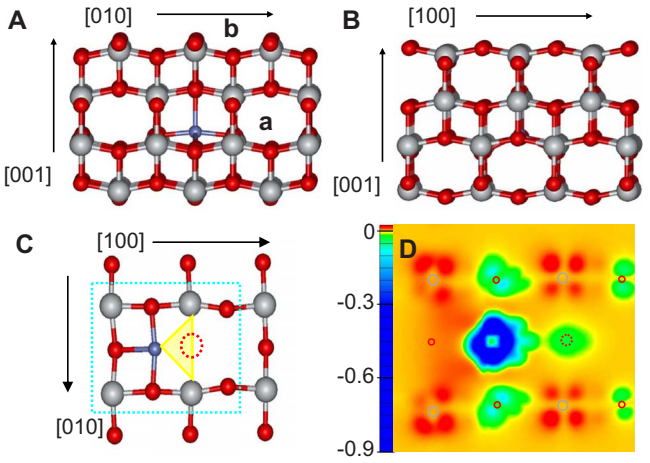


FIG. 4. (Color online) A schematic of the interstitial atomic configuration for a single Co impurity. Ti atoms are shown in gray, O in red, and Co in blue. (a) and (b) correspond to views down the [100] and [010] projections, respectively. In (c) a projection along the [001] axis of the atomic plane where the Co is sitting is shown. The position of the O vacancy has been marked with a red dotted circle. The Co-$Ti^{+3}$-$V_O$ complex is highlighted with a yellow triangle. (d) Contour plots (in arbitrary units) for the difference between the majority- and minority-spin electronic densities in the plane of the Co-$Ti^{+3}$-$V_O$ defect complex [blue box in (c)]. Grey circles mark the position of Ti atoms while red circles mark the O positions, approximately. The blue areas correspond to the maximal negative value of this difference (majority-spin accumulation), which is located mainly at the Co atom. The two surrounding O atoms and the oxygen vacancy (dashed red circle) are also significantly spin polarized. The spin-polarization of the surrounding Ti atoms is much weaker and is opposite in sign (red color).

energy of 1 eV. We infer that postgrowth annealing produces arrays of interstitial Co atoms, each of which is associated with a $V_O$.

Finally, in the absence of $V_O$ we calculated a magnetic moment, $m_{Co} \sim 2.24\mu_B$, per Co atom. When a $V_O$ is adjacent to the interstitial Co, $m_{Co}$ is $\sim 0.9\mu_B$ per atom in fair agreement with the measured value of $0.65\mu_B$. To investigate magnetic ordering of the Co-$V_O$ defect complexes, we placed two such defects in the same supercell at adjacent equivalent columns, as observed in the *Z*-contrast images [e.g., the second atom is placed at points marked a or b in Fig. 4(a), or at site c located below a in the next plane]. The Co-Co distances for such defects pairs are 0.399, 0.537, and 0.564 nm, respectively. In all cases, FM ordering has lower energy than anti-FM ordering with the energy differences being 0.38, 0.24, and 0.22 eV, respectively. FM ordering is preferred even though the atoms along the line connecting Co atoms in the three cases are completely different. As expected, the energy difference decreases with increasing Co-Co distance but cannot be tracked with sufficient accuracy to the mean Co-Co distance at 3 at % doping ($\sim 10$ Å). The evident ordering of Co atoms in only half of equivalent columns suggests an average Co-Co distance that is half the mean value corresponding to 3 at % doping, i.e., about 5 Å. We conclude that DFT and LSDA capture the spin-aligning interactions that lead to FM ordering of the magnetic moments of Co-$V_O$ defects.

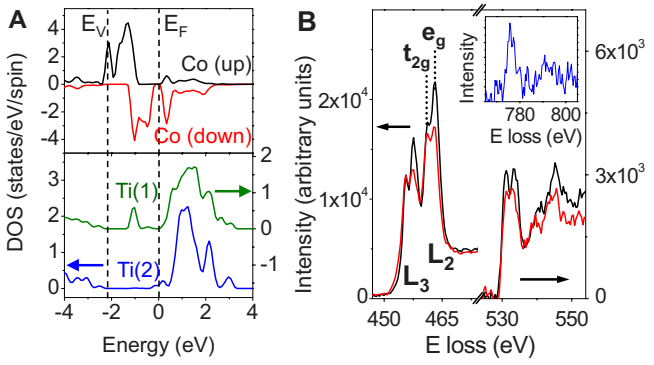


FIG. 5. (Color online) (a) PDOS for the majority (positive) and minority (negative) spin states on the interstitial Co atom in the Co-$Ti^{+3}$-$V_O$ defect complex (upper panel). The lower panel compares the PDOS for the Ti atom by the Co interstitial [green, Ti(1)] with the PDOS for a general Ti atom [blue, Ti(2)] in the anatase lattice. Only one spin component is shown for both Ti atoms (the spin polarization is insignificant). (b) Energy-loss near edge structure at the Ti $L_{2,3}$ edge around 455 eV (left) and the O *K* edge around 530 eV (right) from inequivalent Ti/O atomic columns of an annealed Co:$TiO_2$ sample. The red spectrum was acquired by placing the electron beam on a Ti/O column adjacent to a Co interstitial, such as the one labeled on Fig. 3(a). The spectrum in black comes from a Ti/O column adjacent to a conventional O column (with no Co nearby). A typical example of an averaged EELS Cobalt *L* edge around 779 eV is shown in the inset (total acquisition time of 10 s).

Figure 4(d) shows the difference in spin-up and spin-down total electron densities in the defect complex plane [illustrated in Fig. 4(c)], and confirms that the unpaired spins are located primarily on the Co atom. Projected densities of states (PDOS) show that the unpaired spins originate in defect states within the energy gap. In the absence of $V_O$'s, there are three electrons in the gap states (two spin down, one spin up). When the Co is paired with a $V_O$, we have five electrons in the gap states (three spin down and two spin up). In Fig. 5(a) we plot the PDOS on a Ti atom far from (blue) and next to the Co and $V_O$ (green). The peak in the gap corresponds to roughly an electron in Ti orbitals, suggesting that its "oxidation state" is smaller by one relative to that of the Ti atoms far from the defect ($Ti^{+3}$, as opposed to $Ti^{+4}$). In summary, the results of these calculations together with the *Z*-contrast images suggest that dilute arrays of Co-$Ti^{+3}$-$V_O$ complexes are responsible for ferromagnetism in these systems. The fact that the system is insulating suggests that the annealing process generates only $V_O$'s bound to Co atoms, for which the calculations find no free carriers (in contrast, isolated vacancies generate free carriers with experimental evidence is discussed below, see also Ref. 36).

## V. ATOMIC-RESOLUTION ELECTRON–ENERGY-LOSS SPECTROSCOPY

The presence of Co-$Ti^{+3}$-$V_O$ defect complexes is confirmed by atomic column-by-column EELS measurements. For nonspherical symmetry such as octahedral coordination, the crystal field further splits the $L_3$ and $L_2$ peaks into $t_{2g}$ and $e_g$ levels with relative intensities ($t_{2g}/e_g$) proportional to their

oxidation state.[37] The $L_2$ edge exhibits a more pronounced change in $t_{2g}/e_g$ peak ratio than the $L_3$ edge [see Fig. 5(b)]. A different prepeak splitting is also observed at the O $K$ edge [Fig. 5(b), right].[38,39] A significant decrease in the Ti $L_2$ $t_{2g}/e_g$ ratio was observed from the bright O columns $(0.87 \pm 0.008)$ compared to the dim columns $(0.80 \pm 0.008)$. Therefore, the brighter O columns, with higher Co content, have an increased number of $Ti^{+3}$ nearest neighbors, in good agreement with the theoretical calculations. Note that the EELS analysis of the Ti oxidation state on the atomic columns included an analysis of the Co/Ti ratio, where all columns had a Co concentration falling within the 2–5 at % Co range. The most likely scenario, consistent with the images, the EELS, and the theory, is an ordering of Co interstitials close to the bright O columns with associated $V_O$'s and $Ti^{+3}$ ions, as illustrated in Fig. 4(c).[40] Again, no evidence of defect ordering was found in either the as-deposited $Co:TiO_2$ films or in the annealed, undoped $TiO_2$ films.

Finally, we calculated the $L_{2,3}$ x-ray absorption spectrum of interstitial Co in our Co-$Ti^{+3}$-$V_O$ complex and of substitutional Co, and compared these calculations with the published spectrum[7] of Co in FM 7%-Co-doped anatase (Fig. 6). The calculated spectrum of substitutional Co is in better agreement with the experimental data. The comparison provides further confirmation of our conclusion that Co-$Ti^{+3}$-$V_O$ is the defect responsible for RTFM in Co-doped anatase.

## VI. CONCLUSION

Combining atomic-resolution $Z$-contrast imaging and electron-energy-loss spectroscopy with first-principles density-functional theory and magnetic property measurements, we have shown that the activation of RTFM in highly insulating Co-doped anatase $TiO_2$ is defect mediated and involves the formation of ordered Co-$Ti^{+3}$-$V_O$ defect complexes. The as-deposited Co-doped anatase $TiO_2$ films of this study exhibit only weak RTFM, indicating that a vacuum annealing process is required to form an ordered distribution of defect complexes by the creation and diffusion of $V_O$'s to Co ions. Because undoped anatase $TiO_2$ becomes conducting when annealed, it is clear that O vacancies create carriers. However, the presence of a few atomic percent Co creates a superstructure of specific defect complexes that then trap these carriers and mediate the ferromagnetism.

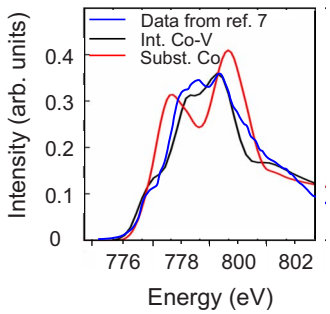


FIG. 6. (Color online) $L_3$ x-ray absorption spectrum of Co in Co-doped anatase (from Ref. 7, in blue), and calculated $L_3$ spectra for Co in the interstitial Co-$Ti^{+3}$-$V_O$ complex (black line) and for substitutional Co (red).

## ACKNOWLEDGMENTS

The authors thank A. Pakhomov for helpful discussions and Kazuo Ishizuka for assistance with data analysis. The work at UW was funded by NSF/ECS Contracts No. 0224138 and No. 0501490 and the Campbell Endowment. Research at ORNL was sponsored by the Office of Basic Energy Sciences, Division of Materials Sciences and Engineering. Research at VU was partially supported by the McMinn Endowment.

*Present address: Idaho National Laboratory. Idaho Falls, Idaho 83415, USA

†Author to whom correspondence should be addressed. kannanmk@u.washington.edu

[1] Y. Matsumoto, M. Murakami, T. Shono, T. Hasegawa, T. Fukumora, M. Kawasaki, P. Ahmet, T. Chikyow, S. Koshihara, and H. Koinuma, Science **291**, 854 (2001).

[2] S. A. Wolf, D. D. Awschalom, R. Buhrman, J. M. Daughton, S. von Molnar, M. L. Roukes, A. Y. Chtchelkanova, and D. M. Treger, Science **294**, 1488 (2001).

[3] H. Ohno, Science **281**, 951 (1998).

[4] T. Dietl, H. Ohno, F. Matsukura, J. Cibert, and D. Ferrand, Science **287**, 1019 (2000).

[5] S. J. Pearton, C. R. Abernathy, M. E. Overberg, G. T. Thaler, D. P. Norton, N. Theodoropolou, A. F. Hebard, Y. D. Park, F. Ren, J. Kim, and L. A. Boatner, J. Appl. Phys. **93**, 1 (2003).

[6] T. Fukumura, Zhengwu Jin, A. Ohtomo, H. Koinuma, and M. Kawasaki, Appl. Phys. Lett. **75**, 3366 (1999).

[7] S. A. Chambers, S. Thevuthasan, R. F. C. Farrow, R. F. Marks, J. U. Thiele, L. Folks, M. G. Samant, A. J. Kellock, N. Ruzycki, D. L. Ederer, and U. Diebold, Appl. Phys. Lett. **79**, 3467 (2001).

[8] T. Dietl, Nat. Mater. **2**, 646 (2003).

[9] J. B. Goodenough, *Magnetism and the Chemical Bond* (Interscience, New York, 1963).

[10] J. M. D. Coey, M. Venkatesan, and C. B. Fitzgerald, Nat. Mater. **4**, 173 (2005).

[11] K. A. Griffin, A. B. Pakhomov, C. M. Wang, S. M. Heald, and Kannan M. Krishnan, Phys. Rev. Lett. **94**, 157204 (2005).

[12] T. Zhao, S. R. Shinde, S. B. Ogale, H. Zheng, T. Venkatesan, R. Ramesh, and S. Das Sarma, Phys. Rev. Lett. **94**, 126601 (2005).

[13] T. Droubay, S. M. Heald, V. Shutthanandan, S. Thevuthasan, S. A. Chambers, and J. Osterwalder, J. Appl. Phys. **97**, 046103 (2005).

[14] S. D. Yoon, Y. Chen, A. Yang, T. L. Goodrich, X. Zuo, K. Ziemer, C. Vittoria, and V. G. Harris, J. Magn. Magn. Mater. **309**, 171 (2007).

[15] P. V. Radovanovic and D. R. Gamelin, Phys. Rev. Lett. **91**, 157202 (2003); K. R. Kittilstved, N. S. Norberg, and D. R.

Gamelin, *ibid.* **94**, 147209 (2005).
[16] J. D. Bryan, S. A. Santangelo, S. C. Keveren, and D. R. Gamelin, J. Am. Chem. Soc. **127**, 15568 (2005); P. I. Archer, P. V. Radovanovic, S. M. Heald, and D. R. Gamelin, *ibid.* **127**, 14479 (2005).
[17] T. C. Kaspar, S. M. Heald, C. M. Wang, J. D. Bryan, T. Droubay, V. Shutthanandan, S. Thevuthasan, D. E. McCready, A. J. Kellock, D. R. Gamelin, and S. A. Chambers, Phys. Rev. Lett. **95**, 217203 (2005).
[18] K. A. Griffin, A. B. Pakhomov, C. M. Wang, S. M. Heald, and Kannan M. Krishnan, J. Appl. Phys. **97**, 10D320 (2005).
[19] K. A. Griffin, M. Varela, S. J. Pennycook, A. B. Pakhomov, and K. M. Krishnan, J. Appl. Phys. **99**, 08M114 (2006).
[20] I. S. Elfimov, S. Yunoki, and G. A. Sawatzky, Phys. Rev. Lett. **89**, 216403 (2002).
[21] C. Das Pemmaraju and S. Sanvito, Phys. Rev. Lett. **94**, 217205 (2005).
[22] K. Kikoin and V. Fleurov, Phys. Rev. B **74**, 174407 (2006).
[23] J. M. D. Coey, Solid State Sci. **7**, 660 (2005).
[24] M. S. Park, S. K. Kwon, and B. I. Min, Phys. Rev. B **65**, 161201(R) (2002).
[25] H. Weng, X. Yang, J. Dong, H. Mizuseki, M. Kawasaki, and Y. Kawazoe, Phys. Rev. B **69**, 125219 (2004).
[26] J. M. Sullivan and S. C. Erwin, Phys. Rev. B **67**, 144415 (2003).
[27] J. E. Jaffe, T. C. Droubay, and S. A. Chambers, J. Appl. Phys. **97**, 073908 (2005).
[28] M. Varela, S. D. Findlay, A. R. Lupini, H. M. Christen, A. Y. Borisevich, N. Dellby, O. L. Krivanek, P. D. Nellist, M. P. Oxley, L. J. Allen, and S. J. Pennycook, Phys. Rev. Lett. **92**, 095502 (2004).
[29] N. D. Browning, M. F. Chisholm, and S. J. Pennycook, Nature (London) **366**, 143 (1993).
[30] B. Rafferty and S. J. Pennycook, Ultramicroscopy **78**, 141 (1999).
[31] L. J. Allen, S. D. Findlay, A. R. Lupini, M. P. Oxley, and S. J. Pennycook, Phys. Rev. Lett. **91**, 105503 (2003).
[32] Y. Ito, R. F. Klie, N. D. Browning, and T. J. Mazanec, J. Am. Ceram. Soc. **85**, 969 (2002).
[33] M. C. Payne, M. P. Teter, D. C. Allan, T. A. Arias, and J. D. Joannopoulos, Rev. Mod. Phys. **64**, 1045 (1992).
[34] G. Kresse and J. Hafner, Phys. Rev. B **48**, 13115 (1993); G. Kresse and J. Furthmüller, *ibid.* **54**, 11169 (1996).
[35] C. G. Van de Walle, D. B. Laks, G. F. Neumark, and S. T. Pantelides, Phys. Rev. B **47**, 9425 (1993).
[36] M. Kim, G. Duscher, N. D. Browning, K. Sohlberg, S. T. Pantelides, and S. J. Pennycook, Phys. Rev. Lett. **86**, 4056 (2001).
[37] M. Abbate, F. M. F. de Groot, J. C. Fuggle, A. Fujimori, Y. Tokura, Y. Fujishima, O. Strebel, M. Domke, G. Kaindl, J. van Elp, B. T. Thole, G. A. Sawatzky, M. Sacchi, and N. Tsuda, Phys. Rev. B **44**, 5419 (1991).
[38] H. Kurata, E. Lefevre, C. Colliex, and R. Brydson, Phys. Rev. B **47**, 13763 (1993).
[39] R. Brydson, H. Sauer, W. Engel, J. M. Thomas, E. Zeitler, N. Kosugi, and H. Kuroda, J. Phys.: Condens. Matter **1**, 797 (1989).
[40] Current experimental limitations preclude us from establishing whether the defect complex is charged or what the exact stoichiometry of the defect complex would be. For charge neutrality, the interstitial Co of +2 charge and the $V_O$ of +2 charge would require an effective charge compensation of −4. This could be achieved by the presence, on average, of 4 $Ti^{+3}$ ions, each of which has a −1 charge with respect to the lattice.